Available online at www.sciencedirect.com
SCIENCE DIRECT®
Geothermics 34 (2005) 3–25
GEOTHERMICS
www.elsevier.com/locate/geothermics

An Automated Well-Test Analysis System (AWTAS)

Michael J. O'Sullivan[a,*], Adrian E. Croucher[a], Errol B. Anderson[b], Tsuneo Kikuchi[c], Osamu Nakagome[d]

[a] *Department of Engineering Science, University of Auckland, Private Bag 92019, Auckland, New Zealand*
[b] *PB Power, GENZL Division, P.O. Box 3935, Auckland, New Zealand*
[c] *New Energy and Industrial Technology Development Organization (NEDO), Sunshine 60 Bldg., 3-1-1 Higashi Ikebukuro, Toshima-ku, Tokyo 170-6028, Japan*
[d] *Geothermal Department, Japan Petroleum Exploration Co. (JAPEX), NYK TENNOZ Building, 2-2-20 Higashi Shinagawa, Shinagawa-ku, Tokyo 140, Japan*

Received 14 August 2003; accepted 20 August 2004
Available online 25 December 2004

Abstract

Traditional methods of well-test analysis are of limited applicability to well-tests carried out in geothermal reservoirs. An automatic well-test analysis system (AWTAS) has been constructed that is based on fast numerical models, rather than the analytical (or semi-analytical) models used in traditional analysis. This approach makes it possible to simulate complex non-isothermal situations, including phase changes. It also allows the use of a broader range of model types. Examples are given which demonstrate the ability of the software to analyse geothermal well tests.

Keywords: Well-test analysis; Geothermal; Modelling; AWTAS

1. Introduction

The physical properties of underground reservoirs are generally determined by analysing the results of well tests. In a typical well test, production or injection is carried out at one well, while fluid properties (usually pressure) are measured either in the same well or

* Corresponding author. Tel.: +64 9 373 7599x8393; fax: +64 9 373 7468
E-mail address: m.osullivan@auckland.ac.nz (M.J. O'Sullivan).

0375-6505/$30.00 © 2004 Published by Elsevier Ltd on behalf of CNR.
doi:10.1016/j.geothermics.2004.08.001

Nomenclature

c	specific heat ($J\,kg^{-1}\,K^{-1}$)
C	compressibility (Pa^{-1})
k	permeability (m^2)
K	thermal conductivity ($W\,m^{-1}\,K^{-1}$)
P	pressure (Pa)
q	mass flux ($kg\,s^{-1}$)
Q	specific mass flux ($kg\,m^{-2}\,s^{-1}$)
S	saturation (dimensionless)
s	skin factor (dimensionless)
t	time (s)
T	temperature (°C)
u	specific energy ($J\,kg^{-1}$)
ν	kinematic viscosity ($m^2\,s^{-1}$)
ϕ	porosity (dimensionless)
ρ	density ($kg\,m^{-3}$)
χ^2	chi-square statistic (dimensionless)

in a different one (in the case of interference tests). The most common types of tests in geothermal reservoirs are drawdown/buildup or injection/falloff tests.

The results of the test are interpreted by proposing a model to represent the system, and finding the model parameters that give the best agreement with the measured data. These parameter values then give estimates of the physical properties (e.g. permeability) of the reservoir.

Traditional methods of well-test analysis, developed for the groundwater and oil industries, involve graphical techniques such as Horner plots or type-curve matching (see Earlougher, 1977, for example). These methods are based on simple reservoir models consisting of a single permeable layer, of constant thickness, extending infinitely in all directions from the well. They make further simplifying assumptions regarding the dependence of fluid properties on thermodynamic conditions, and usually assume simple (e.g. constant) production or injection rates. With these assumptions, analytical solutions, such as the 'Theis curve' (Freeze and Cherry, 1979), can be derived for the pressure response at any point. Plotting the observed data on suitable axes then allows the analysis to be reduced to a linear regression problem.

With the development of computers, it became possible to extend these methods and relax some of their simplifying assumptions. In particular, the use of numerical non-linear regression techniques allowed a wider range of well-test situations to be simulated. One of the most important early papers on the topic was by Earlougher and Kersch (1972). Since then, a number of automated well-test analysis systems have been developed. Some offer a range of different analytical or semi-analytical models, catering for different production or injection regimes and reservoir configurations, with a pre-processing stage to help with

the choice of model (i.e. model recognition). An excellent survey paper by Horne (1994) describes these techniques.

The limitations of existing automated well-test analysis systems become apparent, however, when applied to the analysis of geothermal well tests. In geothermal reservoirs, some of the important assumptions used to derive analytical or semi-analytical model solutions are not satisfied. As geothermal reservoirs are generally non-isothermal, the fluid properties are non-uniform and depend non-linearly on thermodynamic conditions (pressure, temperature, saturation and composition), particularly in the presence of phase changes (boiling and recondensing). Analytical models based on uniform fluid properties can give a reasonable approximation to the behaviour of geothermal reservoirs for simple constant-rate drawdown tests (O'Sullivan, 1987a; Grant and Sorey, 1979). The work of Perrine (1956); Martin (1959); Al-Khalifah et al. (1987) and others has also extended the use of analytical analysis techniques to certain types of multi-phase systems. However, the most common kinds of well-tests for geothermal systems are pressure build-up tests, in which expansion and contraction of boiling gases may occur, or injection-falloff tests, in which there are usually large variations in temperature. Therefore, for most geothermal well tests, analytical or semi-analytical models (and hence existing automated well-test analysis systems) cannot be expected to perform well.

Geothermal reservoir modelling is generally carried out using numerical simulators such as the TOUGH2 (Transport Of Unsaturated Groundwater and Heat) code (Pruess, 1991), which allow the non-linear behaviour of the geothermal reservoir to be more closely reproduced. Several modellers (White, 1995; Finsterle et al., 1997; O'Sullivan et al., 1998; White et al., 1998) have performed automatic calibration of geothermal models using the iTOUGH2 ('inverse TOUGH2') code (Finsterle, 1997). This code uses a non-linear regression technique, very similar to those used by automated well-test analysis systems, to find model parameter values that give the best agreement between model results and measured data (i.e. 'inverse' modelling). It differs, however, in that the model response is calculated not analytically, but numerically, using the TOUGH2 simulator. The flexibility of the iTOUGH2 code means that reservoir models of arbitrary complexity may be used. The downside of this is that setting up a model for even a simple well-test can be time-consuming. Running iTOUGH2 can also be demanding on computational resources and run-time.

The aim of the research described in the present paper is to construct an automatic well-test analysis system (AWTAS) that can be applied to geothermal well tests, by combining the approaches of codes such as AUTOMATE for well-test analysis (Horne, 1995) and numerical inverse reservoir modelling codes such as iTOUGH2 (Finsterle, 1997). To produce an automatic well-test analysis system based on numerically generated model responses, the following major ingredients are essential:

- very fast and accurate numerical generation of the model response
- very fast model fitting
- an easy-to-use graphical interface

The first of these requires the development of fast numerical solvers (see Section 3) and the second requires a robust and fast nonlinear regression technique (see Section 4). Some example tests and applications are given to illustrate the use of the AWTAS software.

2. Test types

Because AWTAS uses a numerical solver to generate the model response, well tests with arbitrary production or injection rates can be analysed- including any of the traditional types of test (e.g. drawdown, buildup, injection/falloff). In addition, tests in which the production or injection rate is not constant but varies arbitrarily with time can also be analysed, as long as time series data for the rates are available.

The use of numerical solvers also makes it possible to analyse tests with non-uniform thermodynamic conditions, including two-phase mixtures of water and steam. In some situations, this makes it possible to extract information that is not obtainable using standard well-test analysis. For example, porosity cannot usually be determined from a standard isothermal well test, as the pressure response is not sensitive to porosity. However, in the presence of enthalpy changes, porosity can significantly affect the model response (O'Sullivan, 1987b), and can therefore be determined using AWTAS.

3. Fast numerical solvers

A number of fast numerical solvers have been developed for AWTAS, all using an integrated finite-difference formulation very similar to that used in TOUGH2 (Pruess, 1991). All AWTAS numerical solvers assume radial symmetry about the active well, which greatly simplifies the model structure and increases execution speed. Time step size control is adaptive and fully automatic (see Appendix A).

The AWTAS solvers need to be very robust. During the model fitting process they are run many times, with different combinations of input parameters chosen by the model fitting algorithm, some of which may be physically unlikely. If numerical exceptions such as floating point errors are generated in a particular model run (often indicating that the current time-step size is too large), it is imperative that the model fitting process as a whole is not halted. The AWTAS code therefore contains extensive pre-emptive error trapping, which returns control to the main time-marching routine and reduces the time step size.

3.1. Single layer numerical solver

This numerical solver makes the further assumption that all flow into the well effectively comes through a single feedzone. This results in a two-dimensional model, consisting of a single layer of porous material situated at the main feedzone of the well.

Because of the assumed radial symmetry, this layer can be represented numerically using a one-dimensional radial model grid, further increasing the model execution speed. The radial grid block sizes were chosen on the basis of an extensive scoping study, simulating a large number of well tests using the TOUGH2 simulator and comparing the results, at different grid resolutions and with analytical or quasi-analytical solutions (O'Sullivan and Pruess, 1980; O'Sullivan, 1981). The resulting 100-block grid design has a high-resolution area immediately outside the wellbore (ten blocks of radial thickness 5 cm). Outside this, the block sizes increase exponentially with radius, each block being 1.2 times the size of its inward neighbour. Testing showed that this grid is fine enough to model two-phase processes

(boiling and condensation) near the wellbore, and the grid is large enough to be effectively infinite acting for single-phase hot-water systems.

The details of the numerical implementation of this fast solver are given in Appendix A. The single layer numerical solver has been used to implement various different models in AWTAS, some of which are described below.

3.1.1. Homogeneous porous layer model

This model assumes a completely homogeneous porous medium throughout the feedzone layer, with the same permeability and porosity assigned to all model blocks. For a constant-rate production test under isothermal conditions, this model gives results approximating those given by the Theis curve. The model has two variable parameters- the permeability and porosity of the feedzone layer- that are varied to maximise agreement between model results and field data.

3.1.2. Fractional dimension (fractal) model

Some researchers (e.g. Barker, 1988; Acuna and Yortsos, 1995; Walker and Roberts, 2003) have suggested that a fractured reservoir can be represented by a 'fractal' or 'fractional dimension' model. The homogeneous porous layer model described above represents a two-dimensional model, in which the volume of the feedzone increases with the square of the radial distance from the wellbore. A one-dimensional model would correspond to a situation where fracturing creates a high permeability 'slot' along which most of the fluid feeding the well flows, and the volume of the feedzone increases linearly with radial distance from the wellbore. A three-dimensional model would correspond to general isotropic fracturing throughout the region surrounding the feed point in the well, so that the volume of the feedzone increases with the cube of the radial distance from the wellbore. In some cases, however, the fracture network feeding the well may have a geometric structure that is somewhere in between these cases, and could be represented by a fractional dimension system where the volume swept out by the fracture system, and the area enclosing it, increase with radial distance from the wellbore at an intermediate rate.

The single layer numerical solver has been used to implement this model in AWTAS. The model takes a continuum approach to representing the fractures, rather than modelling them explicitly. In fact, in the integrated finite difference framework used by AWTAS, the only difference from the homogeneous porous layer model implementation lies in the modified specification of block volumes and interface areas, according to the specified 'fractional dimension' n (see Appendix B).

The variable parameters for this model are the same as those for the homogeneous porous layer model, with the addition of the fractional dimension parameter n, which is allowed to take on any value in the range 1.0–3.0. The integer values $n = 1$, 2, and 3 correspond respectively to the special cases of unidirectional linear flow, two-dimensional (homogeneous porous layer) flow, and spherical flow.

3.1.3. Skin model

The 'skin effect' occurs when there is a zone of altered permeability in the immediate vicinity of the wellbore. The permeability may be decreased by blockage of void space during drilling, or increased by acidisation or stimulation (Horne, 1995). The magnitude of

the skin effect may be characterised by a single non-dimensional 'skin factor' parameter s, defined by

$$s = \left(\frac{k}{k_s} - 1\right) \ln\left(\frac{r_s}{r_w}\right) \tag{1}$$

where k and k_s are the permeabilities of the unmodified porous medium and of the skin zone respectively, r_w is the radius of the wellbore, and r_s is the radius of the skin zone.

For a given skin factor, it is necessary to determine appropriate corresponding values of k_s and r_s, so that the permeability k_s can be assigned to model blocks within a radius r_s of the wellbore. The AWTAS skin model first determines a suitable skin zone radius r_s, chosen to line up with a boundary between two grid blocks. The appropriate value of k_s can then be determined by rearranging Eq. (1). Having assigned the permeabilities to the grid, the single layer numerical solver can be run to calculate the model response.

The variable parameters of the skin model are the unmodified permeability k, the feedzone porosity, and the skin factor s.

3.1.4. Leaky aquifer model

The homogeneous porous layer model represents a 'confined' aquifer, since no flow is allowed through the top or bottom of the feedzone layer. Like the Theis curve, this model gives (for a constant-rate production test under isothermal conditions) pressure results that have no steady state, but continue to fall without limit as long as the wellbore is discharged.

This unphysical behaviour may be avoided by allowing leakage through the top and bottom of the layer. This type of model is not widely used in well-test analysis, firstly because the resulting equations cannot be solved analytically, and secondly because the effect is not important for typical short duration tests. In AWTAS, however, this model may be implemented numerically, simply by adding a pressure-dependent 'leakage' term to the calculation of fluid fluxes. The amount of leakage is proportional to the pressure difference between the feedzone layer and the surrounding aquifer (which is assumed to maintain the pressure initially specified in the feedzone layer). The coefficient of proportionality (the 'leakage coefficient') is treated as a third variable model parameter, along with the feedzone permeability and porosity. This option has proved to be useful in analysing some lengthy tests.

3.1.5. Wellbore storage model

This model was introduced primarily to improve the model fit in injection-falloff tests, where the observed pressures often fall more slowly than predicted by the simple homogeneous porous layer model. The delay effect of storage in the wellbore could potentially account for some of this discrepancy.

To model wellbore storage using the single layer numerical solver, an additional model block is introduced to represent the wellbore. The mass balance equation for this block is then written in a form similar to that of the other model blocks (see Appendix C), so that the single layer numerical solver may still be used. As Appendix C shows, assigning the block the total volume of the wellbore above the feedzone, together with an appropriately large compressibility, allows the wellbore storage process to be modelled in this way.

This approach is an approximate representation of wellbore storage. It could be improved upon by coupling a full wellbore model to the reservoir models included in AWTAS.

The variable parameters for this model are the feedzone permeability and porosity, plus the effective 'wellbore compressibility'.

3.2. MINC solver

The MINC (Multiply INterconnected Continua) approach was introduced by Pruess and Narasimhan (1982) for modelling fractured reservoirs. A generalisation of the 'double porosity' method developed by Warren and Root (1963), MINC represents a fractured reservoir using an idealised system of fracture zones and matrix zones.

The radially symmetric numerical MINC solver included in AWTAS contains a line of fracture blocks (with high permeability and small volume) extending out from the wellbore, through which the main flow takes place. Each fracture block has connected to it a set of matrix blocks (with low permeability and large volume). If it is assumed that there is no radial flow in the matrix blocks, the model grid assumes a 'tree' structure with the matrix 'branches' connected to the fracture 'trunk'. For this type of grid, a special elimination technique can be used to speed up solution of the model equations, reducing them to a form solvable by the single layer solver.

The AWTAS MINC model has four variable parameters: the permeability and porosity for the fracture and matrix blocks, respectively.

3.3. Multi-feedzone solver

In many of the measured data sets used to test AWTAS, the final steady pressure in the wellbore after injection has ceased is different from the initial reservoir pressure. This phenomenon is not reproducible using any of the single-layer or MINC models. However, numerical experiments using a TOUGH2 model indicated that in systems with more than one feedzone, a quasi-steady state with different final pressures can occur after injection.

A multi-feedzone fast solver was therefore implemented in AWTAS. This solver models the wellbore approximately as a vertical column of grid blocks with very high permeability ($\sim 10^{-7}$ m^2) and porosity (0.9–0.99). Representing the wellbore as a porous medium is of course an approximation with only limited validity; however, the errors introduced in representing the frictional forces by Darcy's law are generally not significant, as flows in the wellbore during injection and after it is ceased are dominated by gravity effects.

Each feedzone is represented by a line of radial blocks (very similar to a single layer AWTAS model), connected to one of the wellbore blocks. Between the feedzones there are inactive grid layers representing the surrounding impermeable rock.

The multi-feedzone model grid has a 'tree' structure like that of the MINC model grid, but with the 'trunk' (the wellbore) oriented vertically rather than horizontally. It was therefore possible to construct the multi-feedzone solver by adapting the existing MINC solver. The main numerical difference between the two solvers is in the calculation of vertical fluid fluxes between the wellbore blocks, where it is necessary to include the gravity term in Darcy's law.

Setting up the initial reservoir conditions for the multi-feedzone solver also requires special treatment. For single-layer models, the user needs to specify only the pressure and temperature (or saturation for two-phase conditions) at the feedzone depth. For multi-feedzone models, a downhole temperature profile must be specified, which is interpolated to give values at the grid block layers. An approximate hydrostatic initial pressure profile is then calculated, based on the input temperature profile. This pressure profile is then refined by running the model (with no injection, and with all feedzones rendered inactive) until it reaches steady state. The actual model run can then be carried out, with feedzone layers and injection reactivated.

Using the multi-feedzone solver, it would in principle be possible to allow the user to set up a model with an arbitrary number of feedzones. However, such a model could become slow and complex to use, departing from the original AWTAS concept of using fast, relatively simple numerical models. It was therefore decided to use the solver to implement only a two-feedzone model. This model has a total of four variable parameters: the permeability and porosity of each of the feedzones.

In principle the multi-feedzone model can be used for either production or injection, but the approximate wellbore model is likely to be less accurate for production.

4. Model fitting

AWTAS uses a nonlinear regression technique to find the best-fit variable model parameters for a given set of observation data. The discrepancy between the data and model response is treated as a function of several variables (the variable model parameters) to be minimised. This discrepancy is measured using a 'weighted least-squares error' χ^2 defined by:

$$\chi^2(\mathbf{p}) = \sum_{i=1}^{nd} \left(\frac{d_i - m_i(\mathbf{p})}{\sigma_i} \right)^2 \tag{2}$$

where $\mathbf{p}$ is the vector of variable model parameters, nd is the number of data points, d_i is the ith data point, m_i is the modelled approximation to d_i and σ_i is the estimated measurement error in d_i.

This approach is applicable to any data set (e.g. mixtures of pressure and temperature measurements) and any model type, making it ideal for fitting the numerical models featured in AWTAS. An efficient and robust nonlinear regression algorithm is required to minimise the function $\chi^2(\mathbf{p})$, since this function is relatively time-consuming to evaluate when numerical models are used. AWTAS employs the so-called 'Full Newton' method of Dennis et al. (1981), better known as the 'NL2SOL' algorithm, which is a development of the Levenberg–Marquardt method (Marquardt, 1963) used by the iTOUGH2 package. Both of these methods are specifically designed for least-squares minimisation problems, and the NL2SOL algorithm has attractive efficiency and robustness properties. The algorithm requires the Hessian matrix of the function $\chi^2(\mathbf{p})$ to be calculated, which is carried out using finite difference approximations.

Table 1
Drawdown-buildup test parameters

Parameter	Value
Initial pressure	36 bar
Initial temperature	240 °C
Production rate	50 kg s^{-1}
Duration of drawdown	12 h
Feedzone thickness	100 m
Permeability	10^{-13} m^2
Porosity	0.1

5. Example: drawdown-buildup test; recovery of known parameters

This test uses a synthetic data set to demonstrate the ability of the AWTAS model fitting process to recover known values of variable parameters. First, an AWTAS model was run to generate synthetic data for a geothermal well-test. Random noise was then added to the data, and the model fitting process started from different initial parameter values. The fitted parameter values could then be compared with the known values used to generate the data.

The test used is a drawdown-buildup test in which fluid boils and recondenses, with very non-uniform processes near the wellbore, making analysis by traditional methods impossible. The test is performed in a hot water reservoir with an initial pressure close to the boiling point. During drawdown, the pressure near the wellbore drops below boiling point, and a boiling zone is formed around the wellbore, spreading outwards with time. After the wellbore is shut in, pressures near the wellbore rebound, causing the fluid there to recondense. The boiling zone then forms a ring around the wellbore, which decreases in size over time. When it finally disappears, liquid flows suddenly in towards the wellbore, causing an abrupt jump in pressure.

The main parameters of the test are given in Table 1. The results of numerical simulations of this test using the AWTAS homogeneous porous layer model are shown in Figs. 1–5 .

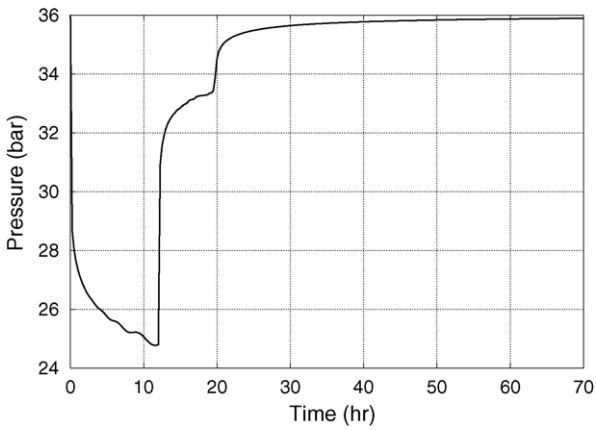

Fig. 1. Modelled pressure results for the drawdown-buildup test.

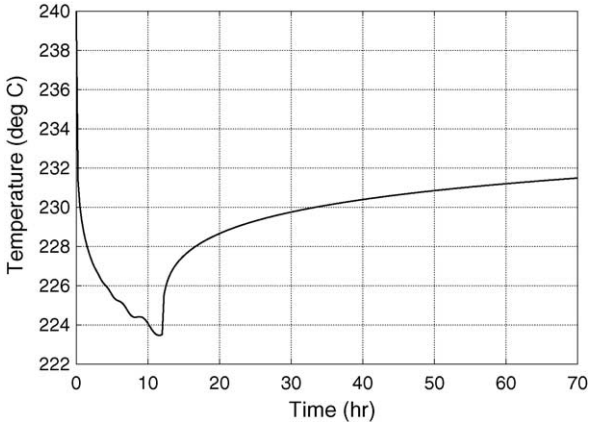

Fig. 2. Modelled temperature results for the drawdown-buildup test.

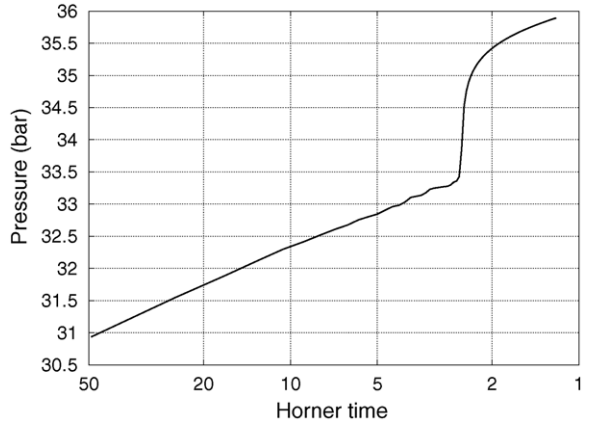

Fig. 3. Horner plot for the drawdown-buildup test.

Figs. 1 and 2 show the modelled pressures and temperatures at the wellbore, respectively. The pressure jump caused by the collapse of the boiling zone during buildup can be clearly seen at around $t = 20$ h. Fig. 3 shows a Horner plot of the pressure buildup. The nonlinear nature of this plot, caused by the phase changes and pressure jump, show the limitations of Horner plot analysis under these conditions.

Gaussian random noise (with standard deviation 0.25 bar for pressure and 0.25 °C for temperature) was added to the above results, and the data fitted using AWTAS. Table 2 gives the initial parameter values and the final fitted parameters, which are very close to the values used to generate the original data. Besides showing the ability of the AWTAS model fitting process to recover the correct parameters, this test also demonstrates that, for well-tests that include significant enthalpy changes, it is possible to determine porosity as well as permeability.

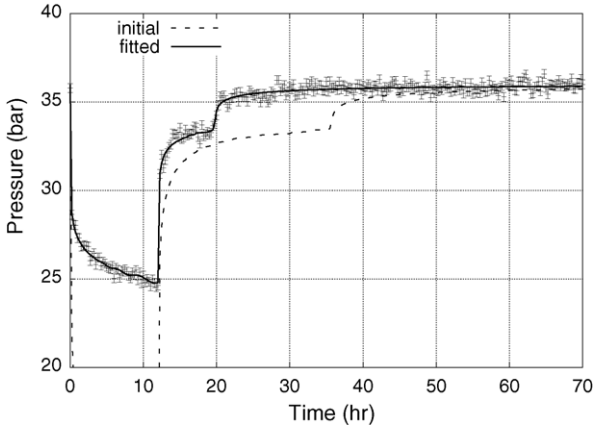

Fig. 4. Fitted pressure results for the drawdown-buildup test.

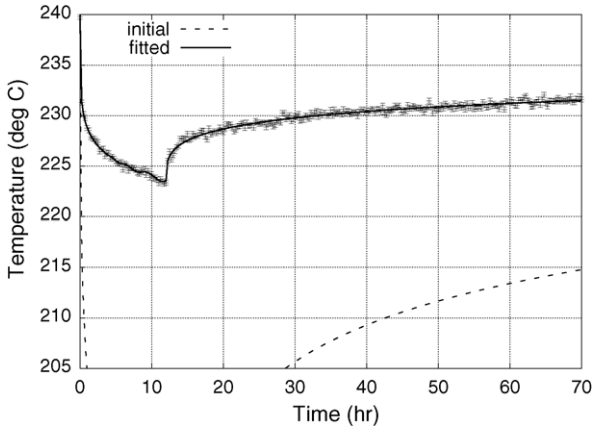

Fig. 5. Fitted temperature results for the drawdown-buildup test.

Figs. 4 and 5 show the synthetic data set (with added noise), together with the model results for both the initial and fitted parameters. The good fit to the data evident from these plots is confirmed by the final χ^2 value given in Table 2. For a good fit, we expect $|m_i - d_i| \sim \sigma_i$, which gives (from Eq. (2)) $\chi^2 \sim nd$. In this case $nd = 578$, so the final χ^2 value of 635 indicates a good fit.

Table 2
Model fitting results for the drawdown-buildup test

Quantity	Initial value	Final value
Permeability	5.0×10^{-14} m^2	9.99×10^{-14} m^2
Porosity	0.15	0.101
χ^2	4.94×10^6	635.0

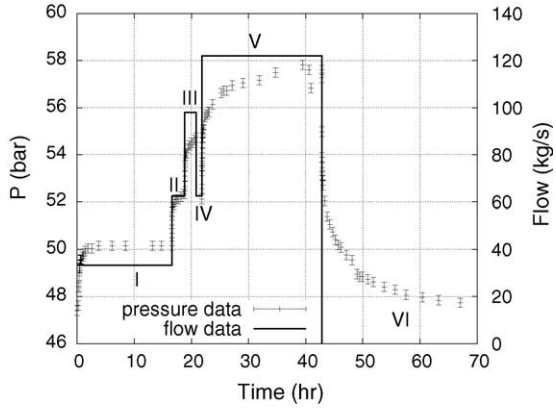

Fig. 6. Flow and pressure data for the multi-rate injection-falloff test.

6. Application: multi-rate injection-falloff test

In this test, cold water (at 20 °C) is injected into a 10 m thick hot (210 °C) reservoir at five different flow rates, and the pressure monitored in the injection well during injection and falloff. The measured pressure data and flow rates are shown in Fig. 6.

For comparison with the AWTAS results, traditional analysis techniques using semi-log plots (Horne, 1994) were used to estimate the permeability-thickness product *kh* for this test. The test was divided into six parts (numbered I–VI in Fig. 6), each with constant flow rate, and the parts analysed individually. In practice, part I did not yield a plot with a straight-line section on either semi-log or log-log axes, and no pressure data were recorded for part IV, so these two parts were excluded from the analysis.

To estimate *kh* from the semi-log plots, the fluid viscosity ν_l is required. Since the injected water is not at the same temperature as the reservoir, it is not clear whether the viscosity of the reservoir fluid ($\nu_l = 1.49 \times 10^{-7}\ m^2\ s^{-1}$) or the injected fluid ($\nu_l = 1.00 \times 10^{-6}\ m^2\ s^{-1}$) should be used, although some authors recommend the use of reservoir fluid properties (Grant et al., 1982). Table 3 shows the calculated values of *kh* for each part of the test, using both values of viscosity (reservoir and injected). The calculated *kh* values vary significantly, the largest (III) being 5.5 times greater than the smallest (V). For non-isothermal tests such as this, we cannot expect reliable results from traditional semi-log analysis.

Fig. 7 shows the results of fitting an AWTAS homogeneous porous layer model to the data. The fit is poor, particularly for the falloff section. This is reflected by the χ^2 value of

Table 3
Results of semi-log analysis for the multi-rate injection-falloff test

Part	Slope (bar/cycle)	Flow rate (kg s^{-1})	*kh* (Reservoir) (m^3)	*kh* (Injected) (m^3)
II	0.55	62.5	3.10×10^{-11}	2.09×10^{-10}
III	0.75	98	3.56×10^{-11}	2.40×10^{-10}
V	3.2	122	1.04×10^{-11}	0.70×10^{-10}
VI	5.15	122	0.65×10^{-11}	0.44×10^{-10}

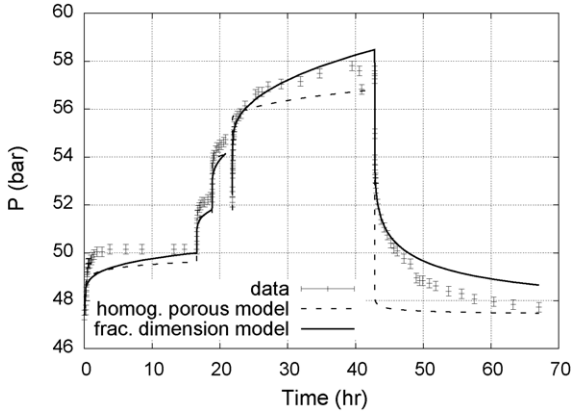

Fig. 7. Fitted pressures for the multi-rate injection-falloff test: homogeneous porous and fractional dimension models.

10263, which is much larger than the number of data points (108). With the assumed layer thickness of 10 m, the fitted *kh* value is 1.37×10^{-10} m^3, which is consistent with the values obtained from the semi-log analysis using the injected fluid viscosity. The fitted porosity is 0.07, but the results are far less sensitive to porosity than to permeability.

Fig. 7 also shows the results of fitting an AWTAS fractional dimension model to this data set. This gives a much improved fit ($\chi^2 = 1277$), though the agreement with the data is still far from perfect, particularly for the first and last sections. The results are very sensitive to fractional dimension (fitted value 1.66), and again, not sensitive to porosity. The fitted *kh* value from this model is 4.05×10^{-10} m^3, which is higher than the values from the homogeneous porous layer model or the semi-log plot analysis. However, as the fractional dimension is not an integer value, the *kh* value from the fractional dimension model is not directly comparable with those obtained from standard two-dimensional models.

7. Application: interference test

In this test, as in the previous one, cold water is injected at varying flow rates into a hot reservoir, but the pressure is monitored at an observation well approximately 35 m away from the injection well. The injected water has enthalpy (100 kJ kg^{-1}) corresponding to an ambient air temperature of approximately 24 °C. The reservoir is initially at a pressure of 85 bar and temperature of 250 °C. The measured flow and pressure data are shown in Fig. 8.

Model fitting was carried out initially using a homogeneous porous layer model, with feedzone thickness of 100 m. The resulting best-fit model parameters and χ^2 value are given in Table 4, and the fitted pressure curve is shown in Fig. 9. Since the number of pressure data is 324, the best-fit χ^2 value of over 20,000 clearly indicates an inadequate fit, given the estimated pressure measurement error $\sigma = 0.01$ bar. The fitted pressure curve undershoots the data near the start and end of the test, and overshoots the measured peak. This indicates that the homogeneous porous layer model is not representing the reservoir adequately.

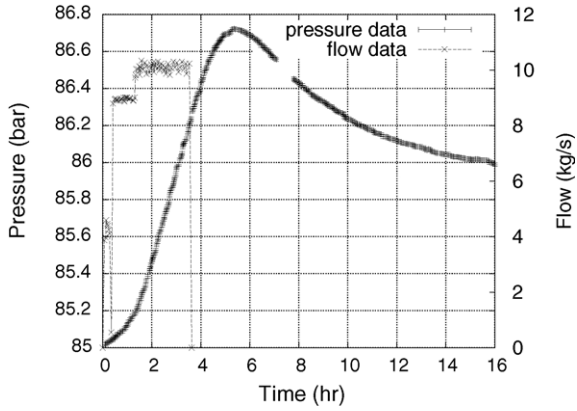

Fig. 8. Flow and pressure data for the interference test.

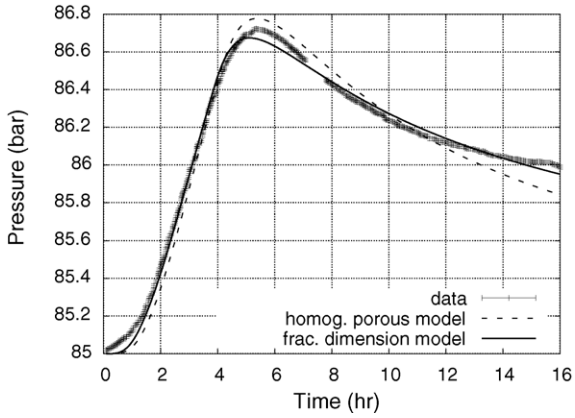

Fig. 9. Fitted pressures for the interference test: homogeneous porous and fractional dimension models.

The model fitting procedure was repeated using a fractional dimension model. The much lower χ^2 value (see Table 4) shows that this model gives a significantly better fit to the data, as confirmed by the pressure plot shown in Fig. 9. The slopes of the pressure buildup and decline are more closely simulated by this model. The fitted fractional dimension of approximately 1.37 suggests the main flow between the two wells may be occurring mainly

Table 4
Model fitting results for the interference test

Quantity	Homogenous porous model results	Fractional dimension model results
Permeability	2.32×10^{-15} m^2	5.10×10^{-15} m^2
Porosity	0.0995	0.1380
Fractional dimension	–	1.3665
χ^2	20,056	3783

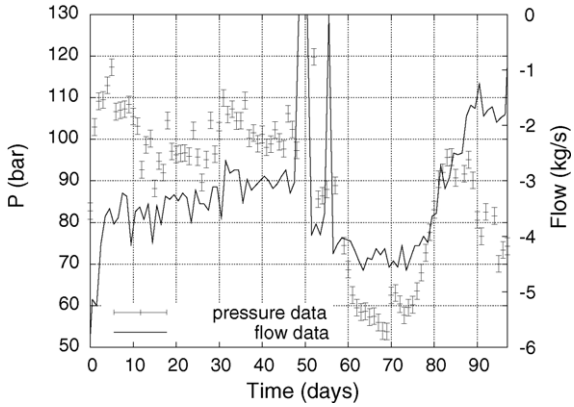

Fig. 10. Flow and pressure data for the two-phase production test.

along a preferred direction, caused by the presence of fractures, rather than equally in all directions from the action well. There are still noticeable discrepancies between the data and the model results, reflected by the fact that the χ^2 value is still an order of magnitude larger than the number of pressure data. However, model fitting using other AWTAS models did not produce results any better than those obtained using the fractional dimension model.

Techniques have been proposed for estimating the fractional dimension using log-log plot analysis of the time derivative of the pressure response (Walker and Roberts, 2003). Because they assume a constant flow rate, however, these techniques are not directly applicable to the present test. In addition, the pressure derivatives must usually be estimated using numerical differentiation, which can give poor results when the pressure data contain noise. Even for the present test, in which the noise level in the pressure data is relatively low, the resulting pressure derivative curve is so noisy that no reliable slope can be derived from it.

8. Application: two-phase production test

This test involves production from a geothermal well and demonstrates the use of AWTAS for matching measured enthalpy transients as well as pressures. The reservoir is two-phase, with an initial temperature of 336 °C. Flow rates vary with time, usually between 3 and 5 kg s^{-1}. The flow rates, together with the measured pressure and enthalpy data, are shown in Figs. 10 and 11.

An AWTAS homogeneous porous layer model was used to analyse this test, with an assumed layer thickness of 200 m. As the initial vapour saturation was unknown (and AWTAS does not allow reservoir conditions to be treated as variable parameters to be fitted), this parameter had to be determined by experiment. Trials indicated that initial vapour saturations of around 0.1 gave the best fit to the data.

Fitting the homogeneous porous layer model to this truncated data set gave permeability and porosity values of $k = 7.27 \times 10^{-16}$ m^2 and $\phi = 0.091$, respectively. The modelled pressure and enthalpy results are shown in Figs. 12 and 13. These results capture the fluctuations

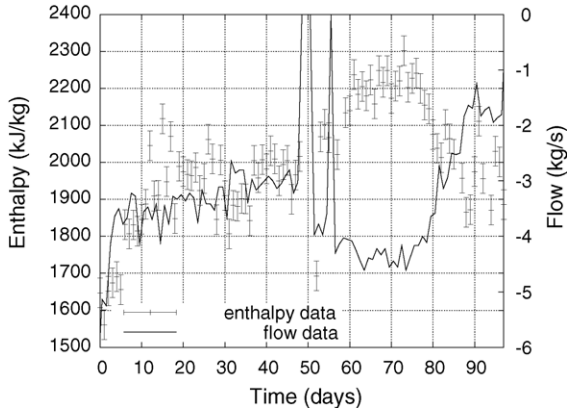

Fig. 11. Flow and enthalpy data for the two-phase production test.

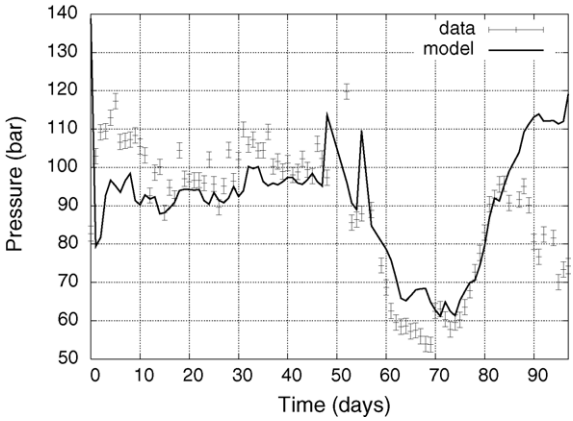

Fig. 12. Fitted pressures for the two-phase production test.

in pressure and enthalpy more closely, with the exception of the early enthalpy data and the pressure drop after 85 days (which is somewhat anomalous, as the production rate over this period is decreasing).

9. Conclusions

An automatic well-test analysis system (AWTAS) has been constructed that is based on the use of numerical models. It is possible, with some simplifying assumptions, to implement numerical models that are fast enough to make this approach practical. The use of numerical models has the advantage that non-isothermal situations, including phase changes, can be simulated, extending the applicability of the software to geothermal well tests. Also, extended tests with complex injection or production histories can be analysed.

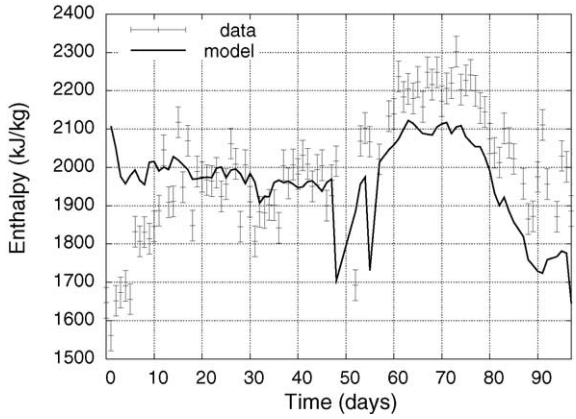

Fig. 13. Fitted enthalpy for the two-phase production test.

AWTAS includes a number of different model types not commonly used in well-test analysis. For some tests, the use of these models (particularly the 'fractional dimension' model for fractured reservoirs) can provide a better match to field data and enhance the physical understanding of the reservoir provided by the well test.

Tests involving significant enthalpy changes can be sensitive not only to permeability but also to porosity. Because it uses numerical models, AWTAS can be used to analyse such tests and hence determine values for porosity.

Acknowledgement

This research was funded by New Energy and Industrial Technology Development Organization (NEDO), and the authors acknowledge the permission of NEDO to publish this paper.

Appendix A. Single layer numerical solver implementation

For a one-dimensional radial model grid, the discrete mass and energy balance equations can be written as

$$V_i\left[M_i^{n+1}-M_i^n\right]+\Delta t^{n+1}\left[FM_{i+1/2}^{n+1}A_{i+1/2}-FM_{i-1/2}^{n+1}A_{i-1/2}\right]=0 \tag{3}$$

and

$$V_i\left[E_i^{n+1}-E_i^n\right]+\Delta t^{n+1}\left[FE_{i+1/2}^{n+1}A_{i+1/2}-FE_{i-1/2}^{n+1}A_{i-1/2}\right]=0 \tag{4}$$

It is an important feature of finite difference formulae (3) and (4) that all the flux terms are evaluated at time t^{n+1}. Such schemes are called "fully implicit". The implicit methods are required in geothermal simulators in order to handle highly nonlinear phase changes.

The quantities in Eqs. (3) and (4) are defined as follows:

i	subscript labelling quantities in block i
$n, n+1$	superscripts labelling quantities evaluated at times t^n, t^{n+1}, respectively
V_i	volume of block i
$A_{i+1/2}$	area of interface between block i and block $i+1$
M_i^{n+1}	mass content per unit volume in block i
E_i^{n+1}	energy content per unit volume in block i
$FM_{i+1/2}^{n+1}$	mass flux between block i and block $i+1$
$FE_{i+1/2}^{n+1}$	energy flux between block i and block $i+1$
Δt^{n+1}	time step between times t^n and t^{n+1}

The mass and energy contents are given in terms of the other quantities by the formulae

$$M_i^n = \phi_i[\rho_{li}^n S_{li}^n - \rho_{vi}^n S_{vi}^n] \tag{5}$$

and

$$E_i^n = (1-\phi_i)\rho_{ri}c_{ri}T_i^n + \phi_i[\rho_{li}^n S_{li}^n u_{li}^n - \rho_{vi}^n S_{vi}^n] \tag{6}$$

where ϕ_i is porosity, ρ_{li}^n is density of water, ρ_{vi}^n is density of steam, S_{li}^n is water saturation (volume fraction), S_{vi}^n is steam saturation, ρ_{ri} is rock density, c_{ri} is rock specific heat, T_i^n is temperature, u_{li}^n is specific energy of water, and u_{vi}^n is specific energy of steam.

These formulae apply for general two-phase conditions (boiling water and steam) and in this case ρ_{li}^n, ρ_{vi}^n, u_{li}^n, u_{vi}^n are all dependent on the pressure p_i^n. Steam table formulae are available for their calculation (see UK Committee on the Properties of Steam, 1970).

The total flow is given as the sum for the individual phases:

$$FM_{i+1/2}^{n+1} = FML_{i+1/2}^{n+1} + FMV_{i+1/2}^{n+1} \tag{7}$$

Here $FML_{i+1/2}^{n+1}$ is the water flux and $FMV_{i+1/2}^{n+1}$ is the steam flux, which are calculated using a two-phase version of Darcy's Law:

$$FML_{i+1/2}^n = -\left[\frac{k\,k_{rl}}{\nu_l}\right]_{i+1/2}^n \frac{p_{i+1}^n - p_i^n}{\Delta r_{i+1/2}} \tag{8}$$

$$FMV_{i+1/2}^n = -\left[\frac{k k_{rv}}{\nu_v}\right]_{i+1/2}^n \frac{p_{i+1}^n - p_i^n}{\Delta r_{i+1/2}} \tag{9}$$

Here $k_{i+1/2}$ is the rock permeability, $k_{rl\,i}^n$ and $k_{rv\,i}^n$ are the relative permeabilities and $\nu_{l\,i}^n$, $\nu_{v\,i}^n$ are the kinematic viscosities of each phase.

Similarly, the total energy flux is given by

$$FE^{n+1}_{i+1/2} = h^n_{li+1/2} FML^n_{i+1/2} + h^n_{vi+1/2} FMV^n_{i+1/2} + K\frac{T^n_{i+1} - T^n_i}{\Delta r_{i+1/2}} \tag{10}$$

Here $h^n_{li+1/2}$ is the enthalpy of water and $h^n_{vi+1/2}$ is the enthalpy of steam.

The last term in Eq. (10) is the energy flux resulting from conduction. The quantity $\Delta r_{i+1/2}$ is the distance between the centres of blocks i and $i+1$, and K is the thermal conductivity.

An important feature of Eqs. (8)–(10) is the evaluation of the interface relative permeabilities, kinematic viscosities and enthalpies. They are calculated using upstream weighting (see Pruess, 1991 or O'Sullivan, 1985).

At the first time step the initial data provide values for $p^0_i \ldots$ and T^0_i (or S^0_{vi}) for $i = 1, 2, \ldots, M$. The boundary conditions must also be specified. It is usually assumed that the model is sufficiently large so that it is "infinite acting" and no flow occurs at the end of the model.

Thus

$$FM^{n+1}_{M+1/2} = 0 \tag{11}$$

$$FE^{n+1}_{M+1/2} = 0 \tag{12}$$

At the well base or sand face end of the model the total flow is specified: thus

$$FM^{n+1}_{1/2} A_{1/2} = QM^{n+1} \tag{13}$$

Here QM^{n+1} is the specified wellbore flow (positive for injection and negative for production). The energy flux is calculated using

$$FE^{n+1}_{1/2} A_{1/2} = h^{n+1}_{\mathrm{f}} QM^{n+1} \tag{14}$$

Here h^{n+1}_{f} is the flowing enthalpy, which is specified as part of the test conditions for an injection test, or is calculated from p^{n+1}_1 and T^{n+1}_1 (or S^{n+1}_{v1}) for production.

The equations provided by (3) and (4) are non-linear. The complete set of equations for all model grid blocks can be written in vector form as

$$\mathbf{F}(\mathbf{X}) = 0 \tag{15}$$

Here $\mathbf{F}$ is a vector of $2M$ equations with the $2i$ – 1st equation given by (3) and the $2i$th equation given by (4). Similarly $\mathbf{X}$ is a vector of $2M$ unknowns with the $2i$ – 1st element p^{n+1}_i and the $2i$th element T^{n+1}_i (or S^{n+1}_{vi}). The system (15) is solved iteratively using the Newton Raphson method.

The $k+1$st estimate of the solution $\mathbf{X}^{k+1}$ is calculated using

$$\mathbf{J}^k \left[\mathbf{X}^{k+1} - \mathbf{X}^k\right] = -\mathbf{F}^k \tag{16}$$

Here $\mathbf{J}^k$ is the Jacobian matrix defined by

$$\mathbf{J}^k_{i,j} = \frac{\partial \mathbf{F}_i(\mathbf{X}^k)}{\partial \mathbf{X}_j} \tag{17}$$

and $\mathbf{F}^k = \mathbf{F}(\mathbf{X}^k)$. The Jacobian derivative entries are calculated numerically using difference approximations (as in TOUGH2; Pruess, 1991).

The process is initiated by using the solutions at time t^n as the first estimate of the solution at time t^{n+1}. If the scheme does not converge, the time step is decreased (see Pruess, 1991). If convergence is reached in a small number of iterations, the time step is increased.

Eq. (16) represents a large system of sparse linear equations. In TOUGH2 there are several methods available for solving them, including conjugate gradient methods such as GMRES and BICGSTAB (Bullivant et al., 1991; Moridis and Pruess, 1997). These methods apply for general models and general sparse structures for **J**. However, careful examination of the Jacobian arising from (3) and (4) shows that it has a very special structure, namely it has at most six non-zero entries in each row. With some simple additions and subtractions the system of equations can be reduced to a pentadiagonal banded form. A special fast linear equation solver (von Rosenberg, 1969) is available for such systems and has been implemented in the AWTAS code.

Appendix B. Fractional dimension model block areas and volumes

For the fractional dimension model in AWTAS, the model grid block volumes and interface areas must be altered according to the specified fractional dimension n. Table 5 gives the formulae for calculating these quantities.

Here it is assumed that the ith block (see Appendix A) with volume V_i is located between radii $r_{i-1/2}$ and $r_{i+1/2}$. The ith interface with area $A_{i+1/2}$ is located between the ith and $i+1$st blocks at a radius of $r_{i+1/2}$. b is the "layer" thickness and α_n is defined by

$$\alpha_n = \frac{2\pi^{n/2}}{\Gamma(n/2)} \tag{18}$$

Table 5
Block volumes and interface areas for the fractional dimension model

Dimension of model	V_i	$A_{i+1/2}$
1	$2b^2(r_{i+1/2} - r_{i-1/2})$	$2b^2$
2	$\pi b(r^2_{i+1/2} - r^2_{i-1/2})$	$2\pi b r_{i+1/2}$
3	$(4\pi/3)(r^3_{i+1/2} - r^3_{i-1/2})$	$4\pi r^2_{i+1/2}$
n	$(\alpha_n b^{3-n}/n)(r^n_{i+1/2} - r^n_{i-1/2})$	$\alpha_n b^{3-n} r^{n-1}_{i+1/2}$

Appendix C. Wellbore storage model mass balance equations

If the density ρ of fluid in the wellbore is assumed approximately constant, then the total mass M of fluid in the wellbore (above the feedzone) is given by

$$M = \phi A h \rho \tag{19}$$

where A is the cross-sectional area of the wellbore, h is the height of fluid in the wellbore above the feedzone, and ϕ is an effective 'porosity' of the wellbore, defined as the fraction of empty space in the volume occupied by the wellbore. In practice this would be very close to 1.0, and given by the square of the ratio of the inside and outside diameters of the wellbore casing.

The mass balance equation for the well over a small time interval Δt can then be written as

$$\Delta\phi\, Ah\rho + \phi A\, \Delta h\, \rho + \phi Ah\, \Delta\rho = q_m\, \Delta t - a\, Q_{mr}\, \Delta t \tag{20}$$

where q_m is the fluid injection rate into the well (kg s^{-1}), a is the area of feedzone open to the wellbore (i.e. the area of the sandface) and Q_{mr} is the mass flow per unit area through the sandface (kg m^{-2} s^{-1}).

Here $\Delta\phi$ and $\Delta\rho$ represent possible changes in the wellbore radius and fluid density respectively. Provided the wellbore is not 'full' (i.e. $h < h_0$, the measured depth to the feedzone), these changes will be very small and the equation will be dominated by the second term, representing the simple change in fluid level in the wellbore. In this case we have

$$\phi A\, \Delta h\, \rho = q_m\, \Delta t - a\, Q_{mr}\, \Delta t \tag{21}$$

The pressure p in the wellbore at the feedzone level is given approximately by the simple hydrostatic equation:

$$p = p_0 + \rho g h \tag{22}$$

where p_0 is atmospheric pressure and g is the gravitational constant (m s^{-2}). Hence the change in the pressure p over the time interval Δt is given by

$$\Delta p = \rho g \Delta h \tag{23}$$

Substituting Eq. (23) into (21) gives

$$\rho\phi A \frac{\Delta p}{\rho g} = q_m \Delta t - a\, Q_{mr} \Delta t \tag{24}$$

or

$$\rho\phi V_0 \frac{1}{h_0 \rho g} \Delta p = q_m\, \Delta t - a Q_{mr} \Delta t \tag{25}$$

where $V_0 = h_0 A$, the total volume of the wellbore above the feedzone.

Eq. (25) is in a form similar to that of the basic mass balance equation for the other AWTAS model blocks:

$$\rho\phi VC\,\Delta p = q_m\,\Delta t - a\,Q_{mr}\Delta t \tag{26}$$

where V is the block volume and C is the rock compressibility. Comparing this with Eq. (25), it can be seen that the wellbore mass balance equation is the same as the mass balance equation for any other block, provided that the wellbore block is assigned:

- an effective volume equivalent to the total volume of the wellbore above the feedzone, V_0 (calculated automatically by AWTAS)
- an effective compressibility given by

$$C_{\text{eff}} = \frac{1}{h_0\rho g} \tag{27}$$

For example, if $h_0 \sim 1000\,\text{m}$, $\rho \sim 1000\,\text{kg m}^{-3}$, and $g \approx 10\,\text{m s}^{-2}$, then the effective compressibility to be assigned to the wellbore block would be $C_{\text{eff}} \sim 10^{-7}\,\text{Pa}^{-1}$. This is several orders of magnitude larger than the values typically assigned to rock compressibility, which are usually $\sim 10^{-10}\,\text{Pa}^{-1}$.

If the well does become 'full' (i.e. $h = h_0$), then Eq. (20) becomes

$$\rho h_0 A\,\Delta\phi = q_m\,\Delta t - a\,Q_{mr}\,\Delta t \tag{28}$$

as the left-hand side mass balance terms are dominated by changes in the effective porosity ϕ. From the compressibility relation

$$\frac{1}{\phi}\frac{\Delta\phi}{\Delta p} = C_r \tag{29}$$

where C_r is the effective compressibility of the well casing and surrounding rock, this gives

$$\rho\phi V_0 C_r\,\Delta p = q_m\Delta t - a\,Q_{mr}\Delta t \tag{30}$$

which again is of the same form as Eq. (26).

References

Acuna, J.A., Yortsos, Y.C., 1995. Application of fractal geometry to the study of networks of fractures and their pressure transient. Water Res. Res. 31 (3), 527–540.

Al-Khalifah, A.A., Aziz, K., Horne, R.N., 1987. A new approach to multiphase well-test analysis. SPE 16743, Proceedings SPE Annual Fall Conference, Dallas, Texas.

Barker, J.A., 1988. A generalized radial flow model for hydraulic tests in fractured rock. Water Res. Res. 24 (10), 1796–1804.

Bullivant, D.P., O'Sullivan, M.J., Zyvoloski, G.A., 1991. Enhancements of the MULKOM geothermal simulator. Proc. 13th New Zealand Geothermal Workshop, University of Auckland, pp. 175–182.

Dennis, J.E., Gay, D.M., Welsch, R.E., 1981. Algorithm 573: NL2SOL—an adaptive nonlinear least-squares algorithm. ACM Trans. Math. Softw. 7 (3), 348–368.

Earlougher, R.C., 1977. Advances in Well-test Analysis, Vol. 5. Society of Petroleum Engineers Monograph, Dallas, Texas.

Earlougher, R.C., Kersch, M.K., 1972. Field examples of automatic transient test analysis. JPT, 1271–1277.

Finsterle, S., 1997. iTOUGH2 User's Guide, Version 3.1. Report LBNL-40400, Lawrence Berkeley National Laboratory, Berkeley, California.

Finsterle, S., Pruess, K., Bullivant, D.P., O'Sullivan, M.J., 1997. Application of inverse modeling to geothermal reservoir simulation. Proc. 22nd Workshop on Geothermal Reservoir Engineering, Stanford University, Stanford, California, pp. 309–316.

Freeze, R.A., Cherry, J.A., 1979. Groundwater. Prentice-Hall, New Jersey.

Grant, M.A., Donaldson, I.G., Bixley, P.F., 1982. Geothermal Reservoir Engineering. Academic Press, New York.

Grant, M.A., Sorey, M.L., 1979. The compressibility and hydraulic diffusivity of a water-steam flow. Water Res. Res. 15 (3), 684–686.

Horne, R.N., 1994. Advances in computer-aided well-test interpretation. JPT, 599–606.

Horne, R.N., 1995. Modern Well-test Analysis, second ed. Petroway Inc., Palo Alto, California.

Marquardt, D.W., 1963. An algorithm for least squares estimation of non-linear parameters. J. Soc. Indus. Appl. Math. 11, 431–441.

Martin, J.C., 1959. Simplified equations of flow in gas drive reservoirs and the theoretical foundation of multiphase pressure buildup analyses. Trans. AIME 216, 309–311.

Moridis, G., Pruess, K., 1997. T2SOLV: an enhanced package of solvers for the TOUGH2 family of codes. Proc. 22nd Workshop on Geothermal Reservoir Engineering, Stanford University, Stanford, California, pp. 295–301.

O'Sullivan, M.J., Pruess, K., 1980. Analysis of injection testing of geothermal reservoirs. Geotherm. Res. Council Trans. 4, 401–404.

O'Sullivan, M.J., 1981. A similarity method for geothermal well test analysis. Water Res. Res. 17 (2), 390–398.

O'Sullivan, M.J., 1985. Geothermal reservoir simulation. J. Energy Res. 9, 319–332.

O'Sullivan, M.J., 1987a. Aspects of geothermal well test analysis in fractured reservoirs. Transp. Porous Med. 2, 497–517.

O'Sullivan, M.J., 1987b. Modelling of enthalpy transients for geothermal wells. Proc. 9th New Zealand Geothermal Workshop, University of Auckland, pp. 121–125.

O'Sullivan, M.J., Bullivant, D.P., Follows, S.E., Mannington, W.I., 1998. Modelling of the Wairakei–Tauhara geothermal system, Proc. TOUGH Workshop '98, Report LBNL-41995, Lawrence Berkeley National Laboratory, Berkeley, California, pp. 1–6.

Perrine, R.L., 1956. Analysis of pressure buildup curves. Drill. Prod. Prac., API, Dallas, 482–509.

Pruess, K., 1991. TOUGH2 – a general purpose numerical simulator for multiphase fluid and heat transfer, Lawrence Berkeley Report No. LBL-29400, Berkeley, California.

Pruess, K., Narasimhan, T.N., 1982. A practical method for modeling fluid and heat flow in fractured porous media. Paper SPE-10509, Proc. 6th SPE Symposium on Reservoir Simulation, New Orleans, Louisiana, USA.

UK Committee on the Properties of Steam, 1970. UK Steam Tables in SI Units. Edward Arnold Publishers Ltd, London.

von Rosenberg, D.U., 1969. Methods for the Numerical Solution of Partial Differential Equations. American Elsevier, New York.

Walker, D.D., Roberts, R.M., 2003. Flow dimensions corresponding to hydrogeologic conditions. Water Res. Res. 39 (12), 1349, doi:10.1029/2002WR001511.

Warren, J.E., Root, P.J., 1963. The behaviour of naturally fractured reservoirs. Soc. Petro. Eng. J., 245–255.

White, S.P., 1995. Inverse modelling of the Kawerau geothermal reservoir. Proc. 17th New Zealand Geothermal Workshop, University of Auckland, New Zealand, pp. 211–216.

White, S.P., Young, R.M., Kissling, W.M., 1998. Using iTOUGH2 to improve geothermal reservoir models, Proc. TOUGH Workshop '98, Report LBNL-41995, Lawrence Berkeley National Laboratory, Berkeley, California, pp. 25–29.